

microRNA-222 Attenuates Mitochondrial Dysfunction During Transmissible Gastroenteritis Virus Infection

Authors

Xiaomin Zhao, Xiangjun Song, Xiaoyuan Bai, Zhanhang Tan, Xuelian Ma, Jianxiong Guo, Zhichao Zhang, Qian Du, Yong Huang, and Dewen Tong

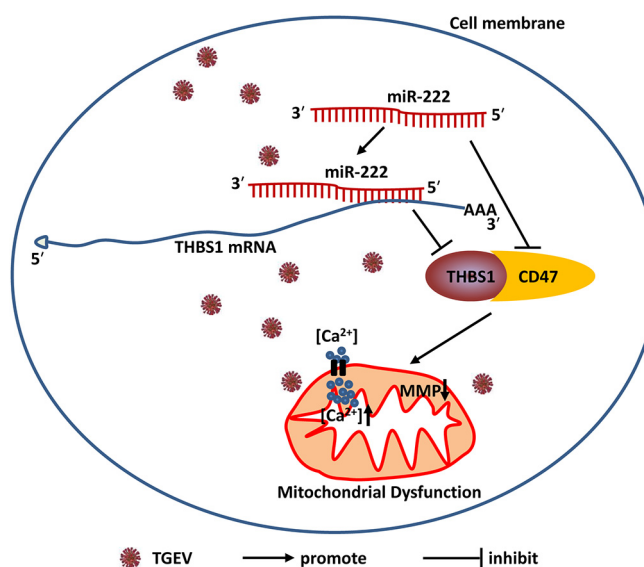
Correspondence

dwtong@nwsuaf.edu.cn

In Brief

Zhao et al. identify microRNA-222 as a mediator of mitochondrial dysfunction, THBS1, and CD47 induced during TGEV infection and showed that microRNA-222 inhibits TGEV-induced mitochondrial dysfunction via targeting and downregulating CD47.

Graphical Abstract



Highlights

- microRNA-222 attenuates TGEV-induced mitochondrial dysfunction.
- microRNA-222 downregulates THBS1 and CD47.
- THBS1 is the target of microRNA-222 during TGEV infection.
- THBS1 and CD47 increase mitochondrial Ca^{2+} level and reduced mitochondrial membrane potential (MMP).



microRNA-222 Attenuates Mitochondrial Dysfunction During Transmissible Gastroenteritis Virus Infection*[§]

Xiaomin Zhao‡, Xiangjun Song‡, Xiaoyuan Bai‡, Zhanhang Tan§, Xuelian Ma‡, Jianxiong Guo‡, Zhichao Zhang‡, Qian Du‡, Yong Huang‡, and Dewen Tong‡[¶]

Transmissible gastroenteritis virus (TGEV) is a member of *Coronaviridae* family. Our previous research showed that TGEV infection could induce mitochondrial dysfunction and upregulate miR-222 level. Therefore, we presumed that miR-222 might be implicated in regulating mitochondrial dysfunction induced by TGEV infection. To verify the hypothesis, the effect of miR-222 on mitochondrial dysfunction was tested and we showed that miR-222 attenuated TGEV-induced mitochondrial dysfunction. To investigate the underlying molecular mechanism of miR-222 in TGEV-induced mitochondrial dysfunction, a quantitative proteomic analysis of PK-15 cells that were transfected with miR-222 mimics and infected with TGEV was performed. In total, 4151 proteins were quantified and 100 differentially expressed proteins were obtained (57 up-regulated, 43 downregulated), among which thrombospondin-1 (THBS1) and cluster of differentiation 47 (CD47) were downregulated. THBS1 was identified as the target of miR-222. Knockdown of THBS1 and CD47 decreased mitochondrial Ca^{2+} level and increased mitochondrial membrane potential (MMP) level. Reversely, overexpression of THBS1 and CD47 elevated mitochondrial Ca^{2+} level and reduced mitochondrial membrane potential (MMP) level. Together, our data establish a significant role of miR-222 in regulating mitochondrial dysfunction in response to TGEV infection. *Molecular & Cellular Proteomics* 18: 51–64, 2019. DOI: 10.1074/mcp.RA118.000808.

Transmissible gastroenteritis virus (TGEV)¹, an enteropathogenic coronavirus, is an enveloped virus with a positive-sense single-stranded RNA genome (1). TGEV infection can cause apoptosis, inflammation, immune response, autophagy (2–4). We reported that TGEV infection could induce cell apoptosis via mitochondria-mediated pathway and caused a decrease of mitochondrial membrane potential, implying that mitochondrial dysfunction occurs (5, 6). Mitochondrion not only plays a vital role in energy production, but also mediates many pathologic processes, including viral infection, inflam-

mation, apoptosis (7). Therefore, TGEV-induced pathologic processes, including apoptosis, inflammation, immune response, autophagy, might be the consequences of mitochondrial dysfunction.

microRNAs (miRNAs) are a class of small non-coding RNA and plays a crucial role in regulating gene expression at post-transcriptional level by specifically binding to 3' UTR of target mRNA (8). miRNAs are involved in regulating many biological processes, including viral infection (9, 10). Moreover, miRNAs are also involved in modulating the mitochondrial functions (11). miR-222 is a miRNA that is overexpressed in several types of cancers and related to mitochondrial function (12). In our previous study, TGEV infection was found to elevate miR-222 level and to cause mitochondrial dysfunction (13, 14). Therefore, we speculate that miR-222 might have an association with TGEV-induced mitochondrial dysfunction.

To verify the hypothesis, Gene Ontology (GO) enrichment analysis and Kyoto Encyclopedia of Genes and Genomes (KEGG) pathway analysis of miR-222 targets were conducted and showed that miR-222 might be implicated in regulation of mitochondrial function. The effect of miR-222 on mitochondrial dysfunction during TGEV infection was measured. Subsequently, relative protein quantification analysis in response to miR-222 was performed and revealed that THBS1 and CD47 were downregulated by miR-222 and related to mitochondria function. THBS1 was identified as the target of miR-222. We examined the effects of THBS1 and CD47 on mitochondrial Ca^{2+} and MMP and found that THBS1 and CD47 were activators of mitochondrial Ca^{2+} levels and inhibitors of MMP. The data show miR-222 prevent TGEV-induced mitochondrial dysfunction via targeting THBS1 and restraining CD47.

EXPERIMENTAL PROCEDURES

Cells, Virus, and Antibodies—PK-15 cells were purchased from ATCC (CCL-33) and grown in Dulbecco's Minimal Essential Medium (DMEM) supplemented with 10% fetal bovine serum (Gibco, New York), 100 IU of penicillin, and 100 mg of streptomycin per ml, at 37 °C in a 5% CO_2 atmosphere incubator. The TGEV Shaanxi strain

From the ‡College of Veterinary Medicine, Northwest A&F University, Yangling, Shaanxi 712100, P.R. China; §Huyi District Center for Animal Disease Control and Prevention, Xi'an, Shaanxi 710300, P.R. China.

Received May 4, 2018, and in revised form, September 13, 2018

Published, MCP Papers in Press, September 26, 2018, DOI 10.1074/mcp.RA118.000808

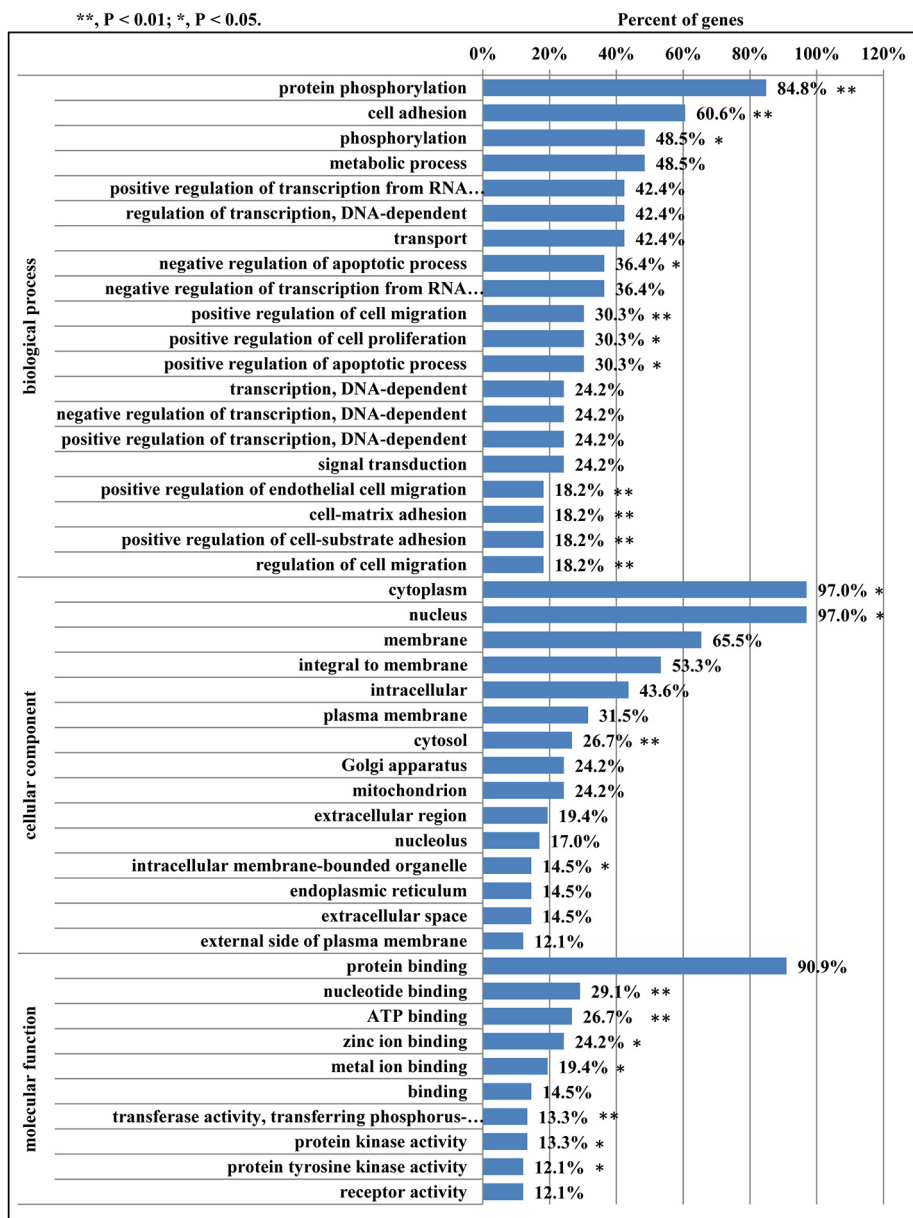


FIG. 1. GO analysis of miR-222 targets. * $p < 0.05$ compared with the control. ** $p < 0.01$ compared with the control.

was isolated from TGEV-infected piglets (15). Anti-THBS1 antibody was obtained from Thermo (Thermo, Waltham, MA). Anti-CD47 antibody was purchased from Abcam (Abcam, Cambridgeshire, UK). The monoclonal β -actin was purchased from Santa Cruz Biotechnology (Santa Cruz).

Experimental Design and Statistical Rationale for Proteomics—To investigate the effect of miR-222 on TGEV-induced mitochondrial dysfunction, PK-15 cells were transfected with miR-222 mimics (experimental samples) or mimics control (control samples) using Lipo-

fectamine 3000 and infected with TGEV at an MOI of 1.0 at 24 h post-transfection (hpt). The cells were collected for quantitative proteomic analysis at 24 h postinfection (hpi). Two biological replicates preparations labeled with TMT were analyzed. The two control samples, which were transfected with miRNA mimics control and infected with TGEV, were respectively labeled with TMT-126 and TMT-129. The two experimental samples, which were transfected with miR-222 mimics and infected with TGEV, were respectively labeled with TMT-128 and TMT-131. To assess the transfection

¹ The abbreviations used are: TGEV, transmissible gastroenteritis virus; PK-15 cells, porcine kidney (PK) 15 cells; PCR, polymerase chain reaction; miRNA, microRNA; THBS1, thrombospondin-1; CD47, cluster of differentiation 47; MMP, mitochondrial membrane potential; qRT-PCR, quantitative reverse transcription PCR; UTR, untranslated region; GO, gene ontology; KEGG, Kyoto encyclopedia

of genes and genomes; MOI, multiplicity of infection; TMT, tandem mass tags; AGC, automatic gain control; hpi, hours post-infection; hpt, hours post-transfection; HPLC, high performance liquid chromatography; MS, mass spectrometry; LC/MS, liquid chromatography-mass spectrometry; LC-MS/MS, liquid chromatography-tandem mass spectrometry.

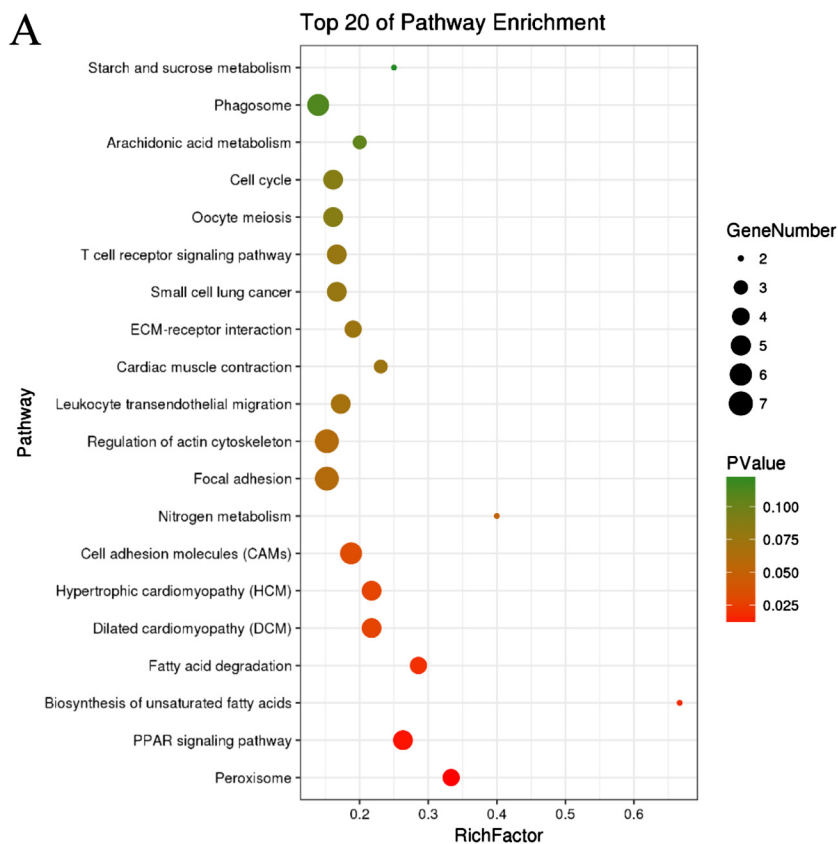
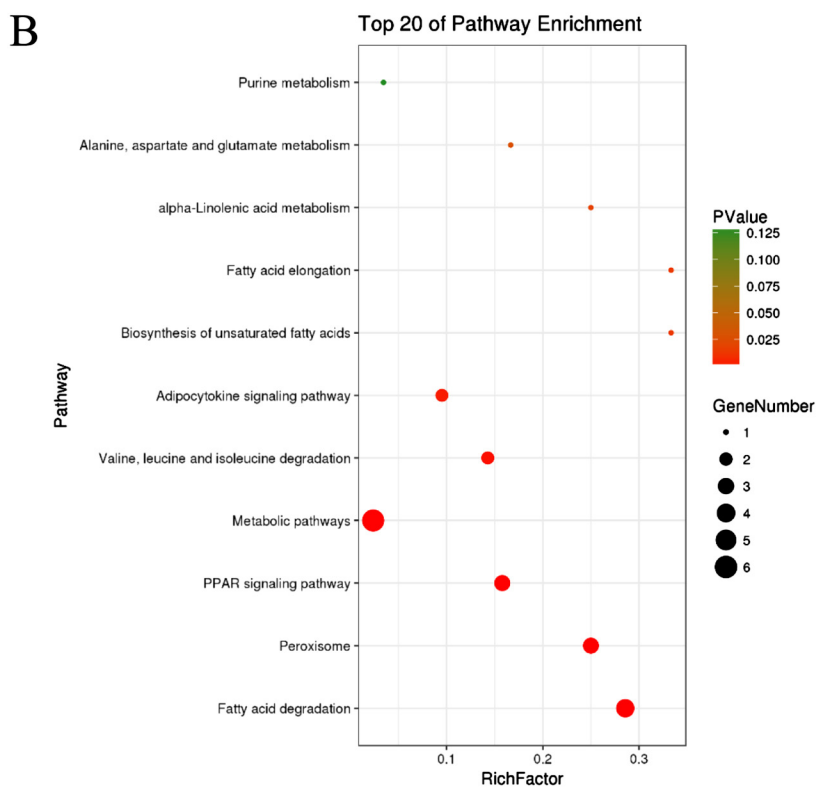


FIG. 2. KEGG analysis of miR-222 targets. A, KEGG analysis for targets of miR-222; B, KEGG analysis for mitochondria-associated targets of miR-222.



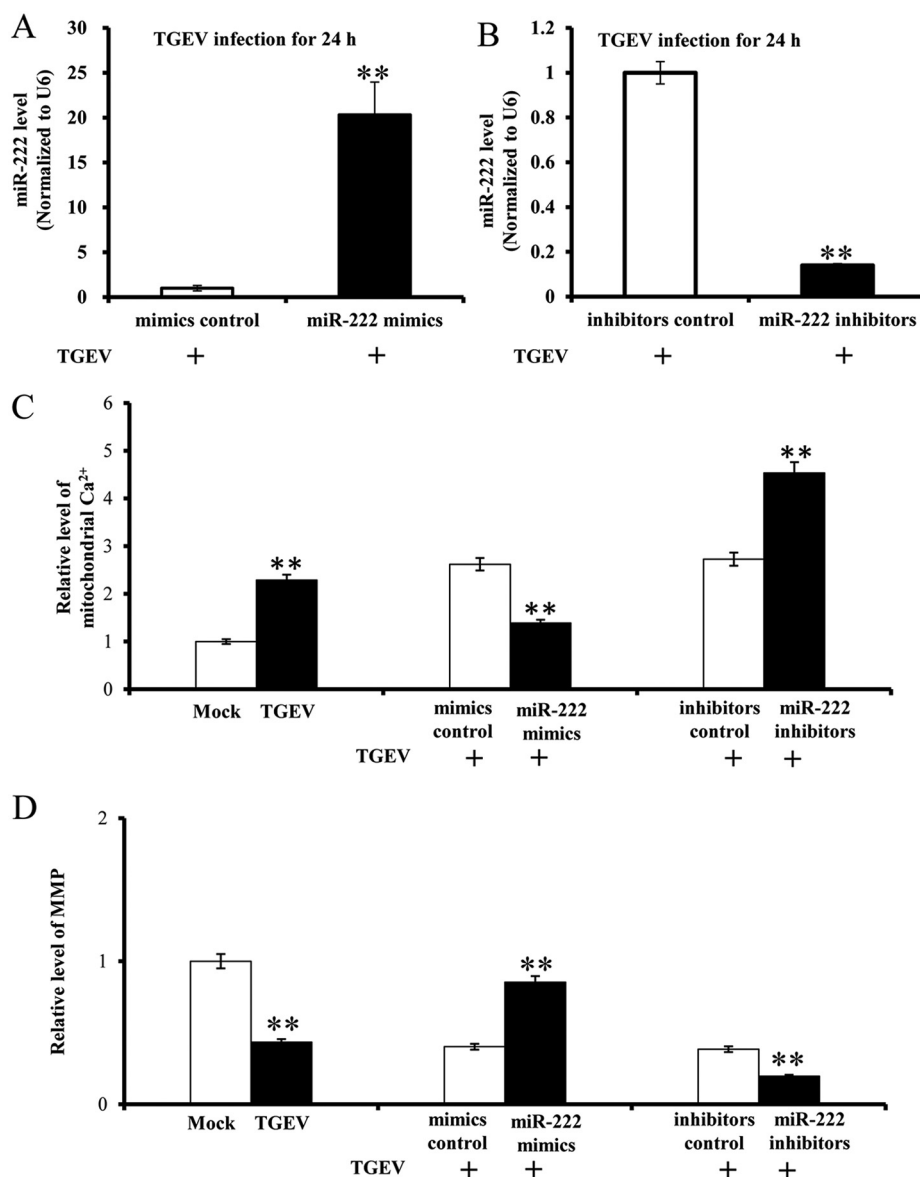


FIG. 3. The effect of miR-222 on TGEV-induced mitochondrial dysfunction. *A*, Overexpression of miR-222 by miR-222 mimics; *B*, Silencing of miR-222 by miR-222 inhibitors; *C*, The effect of miR-222 on mitochondrial Ca²⁺ during TGEV infection; *D*, The effect of miR-222 on MMP during TGEV infection.

efficiency, miR-222 level was measured by qRT-PCR. The sequences of miR-222 mimics, mimics control, and primers are shown in supplemental S1.

Quantification of miRNA and mRNA by qRT-PCR—Total RNA was isolated using Trizol reagent (Invitrogen, California) from PK-15 cells. qRT-PCR was performed as previously described (13). 2 μg of total RNA was treated with DNase I (Fermentas, Germany) for 30 min at 37 °C and reversely transcribed using the First-strand cDNA synthesis kit (Invitrogen). The cDNA was used as the template for qRT-PCR. qRT-PCR was performed using the AccuPower 2×Greenstar qPCR Master mix (Bioneer, Korea) on Bio-Rad iQ5 Real-Time PCR System (Bio-Rad). The relative fold changes of miRNA and mRNA were calculated using two-ddCt method (respectively normalized to U6 and β-actin) (16). The primers are shown in supplemental S1.

Protein Isolation and Labeling with TMT Reagents—Samples were sonicated three times on ice in lysis buffer (8 M urea, 1% Triton-100, 65 mM DTT and 0.1% Protease Inhibitor Mixture) and centrifuged at 20,000 × g at 4 °C for 20 min. The supernatant was treated with cold

15% trichloroacetic acid (TCA) for 2 h at −20 °C and centrifuged for 10 min at 20,000 × g at 4 °C. The precipitate was washed with cold acetone for three times. The protein was dissolved in buffer (8 M urea, 100 mM TEAB, pH 8.0) and concentration was determined with 2-D Quant kit according to the manufacturer’s instructions. 100 μg protein for each sample were digested with trypsin for following experiments. The two control samples transfected with miRNA mimics control was respectively labeled with TMT-126 and TMT-129. The two experimental samples treated with miR-222 mimics were respectively labeled with TMT-128 and TMT-131.

LC-MS/MS Analysis—The samples were fractionated by high pH reverse-phase High Performance Liquid Chromatography (HPLC). Briefly, peptides were dried by vacuum centrifugation, dissolved in 0.1% formic acid, and then directly loaded onto a reversed-phase pre-column (Acclaim PepMap 100), (Thermo Fisher Scientific, Waltham, MA) Subsequently, peptides were separated using a reversed-phase analytical column (Acclaim PepMap RSLC) (Thermo Fisher Scientific) and analyzed by Q Exactive™ hybrid quadrupole-Orbitrap mass spectrometer (Thermo Fisher Scientific).

TABLE I
Differentially expressed proteins induced by overexpression miR-222 mimics in PK-15 cells during TGEV infection^a

No.	Protein name	Fold change	p value	No.	Protein name	Fold change	p value
1	YWHAQ	2.177	0.0346989	51	STAT2	1.215	0.0014066
2	GBP1	2.131	2.094E-08	52	RPS20	1.215	0.0453924
3	SDC4	1.859	0.0042522	53	SMARCA2	1.212	0.0103799
4	MRPL38	1.527	0.044407	54	CNPY2	1.212	0.0229731
5	MRPL47	1.518	0.0138218	55	SERPINB8	1.21	0.0153453
6	MRPL11	1.4485	0.0016448	56	NUB1	1.204	0.0475958
7	CDH1	1.432	0.0046425	57	STX12	1.2015	0.0159419
8	P4HA1	1.41	0.0009798	58	FN1	1.201	1.251E-07
9	CASP4	1.403	0.0189837	59	MYL12B	0.833	2.194E-05
10	HK2	1.394	3.612E-05	60	THBS1	0.832	0.0491643
11	MRPL24	1.39	0.0079873	61	WDR11	0.8305	0.009389
12	BST2	1.383	1.462E-05	62	RRBP1	0.829	0.0029895
13	LAMA3	1.371	0.0374052	63	EIF3H	0.827	5.491E-05
14	CCL5	1.37	0.0087035	64	CDK6	0.826	0.0472265
15	MRPL46	1.366	0.0145114	65	MYH9	0.826	2.689E-14
16	NDUFB5	1.354	0.0151887	66	THOP1	0.8235	0.0014235
17	GVIN1	1.351	0.0046014	67	HEATR5B	0.8235	0.037828
18	MNDA	1.344	0.0018819	68	S100A5	0.82	0.0003203
19	NDUFV1	1.335	0.0424156	69	MRI1	0.818	0.0221039
20	NDUFC2	1.326	0.0487252	70	CAV1	0.8165	0.0001134
21	TACSTD2	1.3095	0.0044767	71	PEA15	0.815	0.0204468
22	RPL34	1.309	0.0314898	72	STAU1	0.813	0.0442707
23	WARS	1.307	5.214E-07	73	CD47	0.811	0.0336522
24	HMGCS1	1.304	0.0011961	74	AHSA2	0.81	0.0066613
25	HINFP	1.296	2.42E-07	75	KRT74	0.81	0.0281688
26	CCN2	1.287	0.0453662	76	FXR2	0.8095	0.0217135
27	SEC61B	1.2865	0.0027047	77	PSD4	0.809	0.0033331
28	HSPG2	1.278	0.0041966	78	ARHGEF1	0.8085	0.0217513
29	ZRANB2	1.2775	0.035522	79	DOCK7	0.808	2.119E-07
30	SNRNP70	1.275	4.575E-05	80	NMT1	0.804	0.0365022
31	MRPS26	1.27	1.605E-05	81	SUMO2	0.8015	0.0095957
32	IRG6	1.2675	4.488E-05	82	M6P/IGF2R	0.8	0.0004368
33	IFIT3	1.261	2.458E-12	83	PTBP2	0.797	0.0282061
34	RAB34	1.254	0.0173716	84	TTYH2	0.795	0.0143047
35	RALB	1.2495	0.0038273	85	AHNAK	0.793	4.937E-15
36	NDUFS1	1.247	0.0078359	86	PBDC1	0.785	0.0241577
37	TMPO	1.2465	0.0148787	87	NLE1	0.782	0.0169835
38	TOP1	1.242	1.734E-05	88	DDI2	0.775	0.0012816
39	IL1RN	1.241	0.0290372	89	SAMD9	0.7745	0.006346
40	TMED5	1.241	0.0147443	90	KTN1	0.772	1.748E-05
41	MCCC2	1.2405	0.0436083	91	TRIO	0.7715	0.0069649
42	SNRPD2	1.2395	0.0006629	92	CALU	0.764	0.0011378
43	RPL14	1.233	0.0018615	93	RPS9	0.757	9.28E-06
44	NDUFA13	1.231	0.0047714	94	RCN1	0.756	0.0338862
45	Ribosomal protein S2	1.227	0.0198054	95	SUN2	0.754	0.0073054
46	MRPS2	1.227	0.0222525	96	TAGLN	0.7365	0.0074309
47	CTDSPL2	1.225	0.0118196	97	KIAA1468	0.7355	0.0468494
48	COX4I1	1.22	6.647E-06	98	STMN1	0.7325	0.01509
49	FKBP9	1.2195	0.0304301	99	TPM1	0.717	0.0007421
50	IFIT2	1.2155	5.104E-05	100	RANBP1	0.676	0.0491162

^aMore information is available in [supplemental S4](#).

The peptides were subjected to NSI source followed by tandem mass spectrometry (MS/MS) in Q Exactive™ (Thermo Fisher Scientific) coupled online to the HPLC. Intact peptides were detected in the Orbitrap at a resolution of 70,000. Peptides were selected for MS/MS using NCE setting as 32. Ion fragments were detected in the Orbitrap at a resolution of 17,500. A data-dependent procedure that alternates between one MS scan followed by 20 MS/MS scans was applied for the top 20 precursor ions above a threshold ion count of 2E4 in the MS survey scan

with 30.0 s dynamic exclusion. The electrospray voltage was 2.0 kV. Automatic gain control (AGC) was set at 5E4. For MS scans, the m/z scan range was 350 to 1800. Fixed first mass was set as 100 m/z.

Analysis of LC-MS/MS Data—MS/MS data were analyzed using Mascot search engine (version 2.3.0) following a previously described protocol (17). Briefly, raw MS data files were processed using the LC/MS software Proteome Discoverer (version 1.3.0.339) (Thermo Fisher Scientific) and converted into the Mascot generic format (mgf)

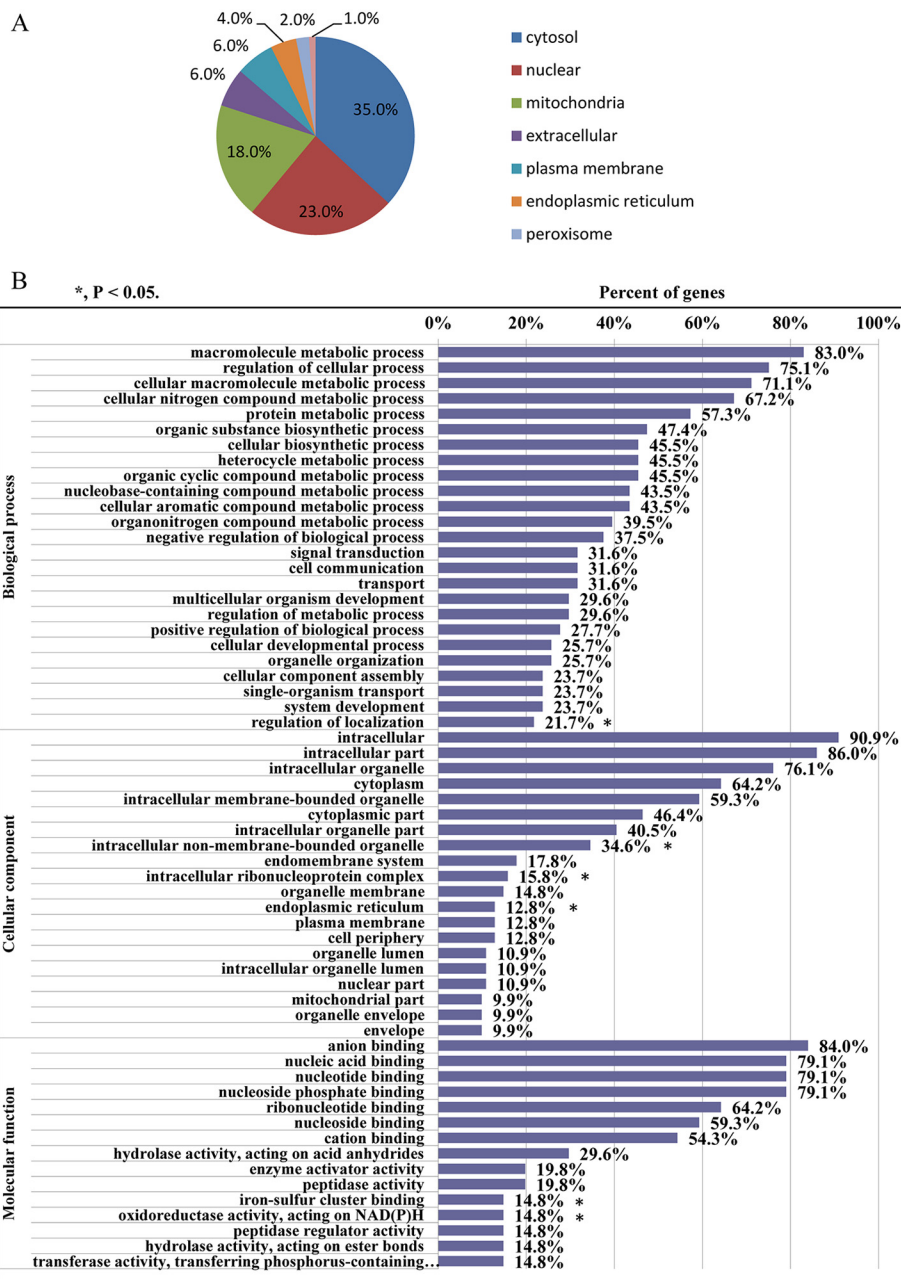


FIG. 4. Subcellular localization and GO analysis of 100 differentially expressed proteins caused by miR-222 overexpression. A, Subcellular localization of differentially expressed proteins caused by miR-222 overexpression; B, GO enrichment analysis of differentially expressed proteins caused by miR-222 overexpression.

files. Mascot software performed peak generation, precursor mass recalibration, extraction of TMT 6-plex reporter ions intensity, and calculation of TMT 6-plex reporter ions intensity ratios. For each MS/MS spectra, top 10 most intense peaks in every 100 Da window were extracted for database search. Then Tandem mass spectra data were searched against Uniprot_Sus scrofa database (UniProt release 2015_04, 26054 sequences) (<http://www.uniprot.org>) concatenated with reversed decoy database and protein sequences of common contaminants using Mascot. Cleavage enzyme was specified as trypsin/P. Maximum number of missing cleavages was set to 2. Mass tolerance for precursor ion was set to 10 ppm and mass tolerance for MS/MS ions was set to 0.02 Da. Carbamydomethylation on Cys, TMT6plex (N-term), and TMT6plex (K) were specified as fixed modification and oxidation on Met. Acetylation on protein N-terminal were specified as variable modifications. False discovery rate (FDR) thresh-

olds for protein, peptide, and modification site were specified at 1%. Mascot software was used to assemble the peptide/protein groups, calculate false discovery rates, and filter the identifications. Protein quantification was set to use only unique peptides bearing any modification. The median ratio of TMT 6-plex reporter intensity of unique peptides was set as protein relative abundance changes. In this study, we prepared two duplicate samples. For each protein, we set the average ratio calculated from two duplicate samples as the final quantitation of protein. Student's test was exploited to calculate differential significance degree of protein relative abundance changes. A fold change >1.2 or < 0.83, plus a p-Value <0.05 (t test), were set as thresholds for significant up and downregulation, respectively. The mass spectrometry proteomics data have been deposited to the ProteomeXchange Consortium via the PRIDE partner repository with the dataset identifier PXD010927 (<http://www.ebi.ac.uk/pride>) (18).

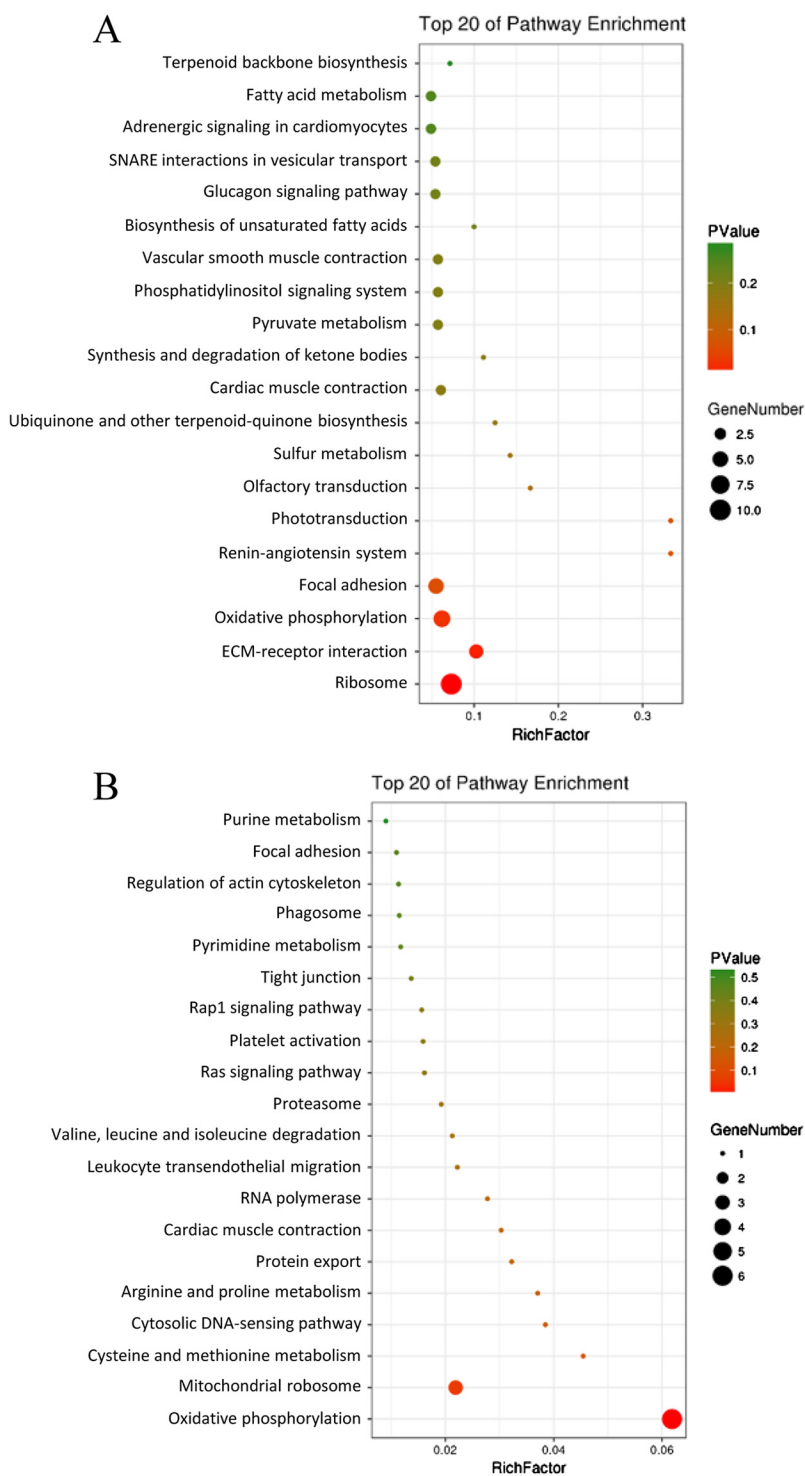


FIG. 5. KEGG analysis of differentially expressed proteins caused by miR-222 overexpression. A, KEGG analysis for differentially expressed proteins; B, KEGG analysis for mitochondria-associated differentially expressed proteins.

GO and KEGG Analysis of Differential-Expressed Proteins—GO annotations of proteome were derived from the UniProt-GOsA database (<http://www.ebi.ac.uk/GOA>). KEGG database was used to annotate proteins pathways. The Wolf Psort database (<https://wolfsort.hgc.jp/>) was used to predict subcellular localization.

Protein-Protein Interaction Analysis—All differentially expressed protein identifiers (Uniprot accession) were searched against STRING database (version 10.0) for protein-protein interactions (19).

Vector Construction—To overexpress THBS1 and CD47, the full-length sequences of THBS1 and CD47 were obtained by PCR from PK-15 cells and cloned into plasmid pCI-neo (Promega). The constructions were respectively named pCI-neo-THBS1 and pCI-neo-CD47. The primer sequences are shown in supplemental S1.

Measurement of Mitochondrial Ca²⁺ Level—Mitochondrial Ca²⁺ level was assessed using Rhod-2 kit (GENMED, China) following the manufacturer’s instruction. Briefly, after being washed, the PK-15

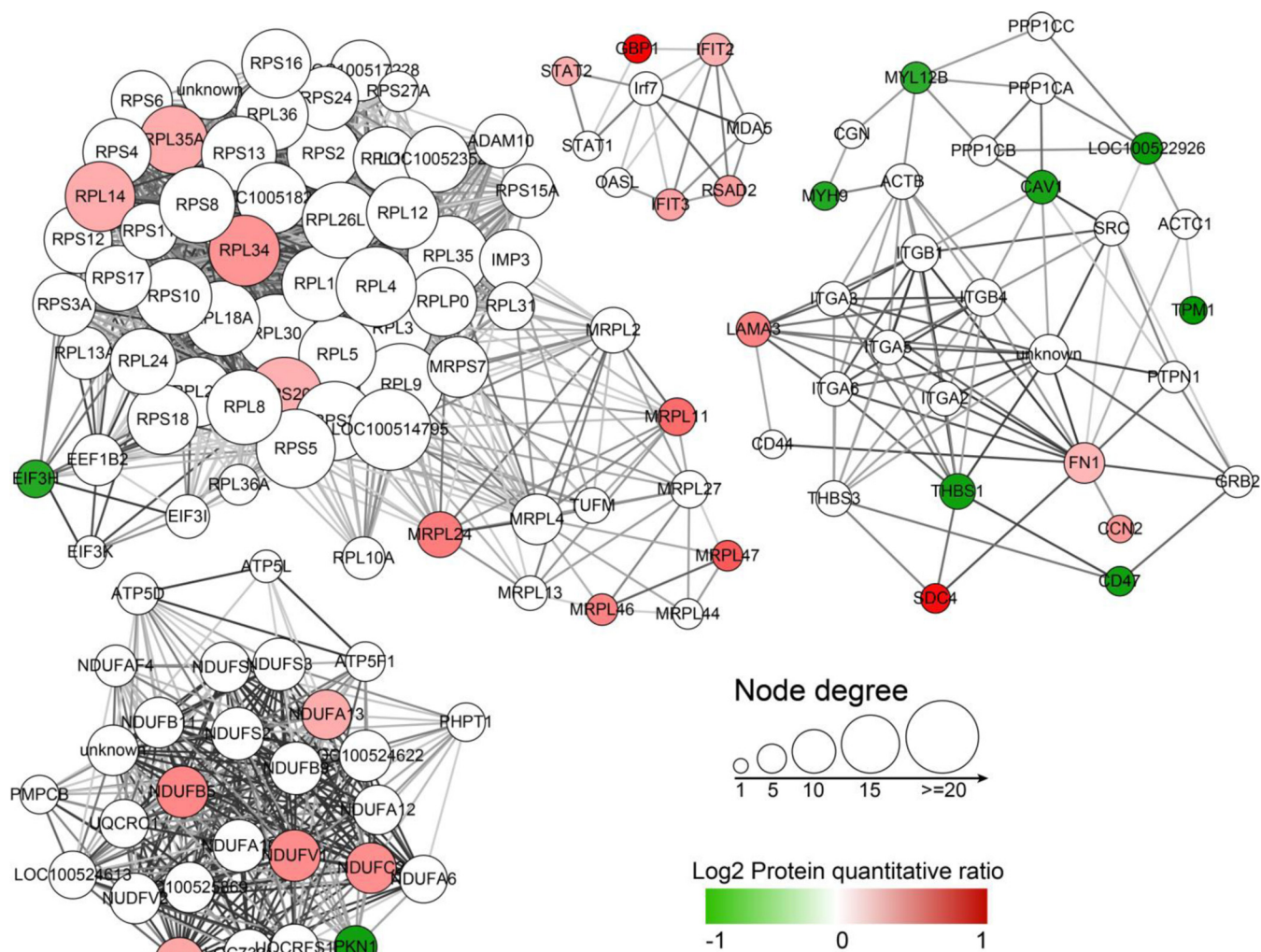


FIG. 6. **Protein-protein interaction networks analysis.** The significantly upregulated proteins are shown in red; The significantly down-regulated proteins are in green.

cells were dyed using dye reagent containing Rhod-2 for 30 min at room temperature and then incubated for 30 min at 37 °C in dark places. The absorbance was measured at 550 ex/590 em using fluorescence spectrophotometer. The relative fluorescence unit (RFU) was calculated according the manufacturer’s instruction.

Evaluation of MMP—MMP of PK-15 cells was assessed using JC-1 kit (GENMED, China) following the manufacturer’s protocol. PK-15 cells were treated with dye reagent containing JC-1 and incubated at room temperature for 10 min. The absorbance was measured at 490 ex/590 em using fluorescence spectrophotometer. The relative fluorescence unit (RFU) was calculated according the manufacturer’s instruction.

Western Blot Analysis—Cells were treated with RIPA lysis buffer containing phenylmethyl sulfonyl fluoride (PMSF). Total proteins were separated on a 12% sodium dodecyl sulfate-polyacrylamide gel electrophoresis (SDS-PAGE) and subsequently transferred onto polyvinylidene difluoride (PVDF) membranes (Millipore). The membrane was blocked with 5% BSA for 2 h at room temperature and successively incubated with primary antibody overnight at 4 °C and with HRP-conjugated secondary antibody at room temperature for 1 h. The signal was detected using enhanced chemiluminescence (ECL) kit (Bio-Rad).

Identification of miR-222 Target—3’ UTRs of 9 candidate target genes, which are related to mitochondria and contain the binding site of miR-222, were respectively amplified by PCR and cloned into dual-luciferase reporter vector, psiCHECK-2 (Promega), to obtain the recombinant plasmids for wildtype of targets. The binding sites of miR-222 in 3’ UTR of targets were mutated following a mutagenesis protocol to obtain the mutants of targets. The primer sequences are shown in [supplemental S1](#). miR-222 mimics, miRNA mimics control, miR-222 inhibitors, and miRNA inhibitors control were synthesized by Ribo Biotech (RiboBio, China) (The sequences are shown in [supplemental S1](#)). PK-15 cells were grown in 24-well plate and then co-transfected with recombinant plasmids for wildtype (or mutant) and miR-222 mimics (or miR-222 inhibitors) using Lipofectamine 3000 (Invitrogen). Luciferase activities were measured on luminometer using Dual-Glo Luciferase Assay System (Promega) following the manufacturer’s manual.

RESULTS

Gene Ontology Enrichment Analysis of miR-222 Targets—TargetScan and miRanda were used to predict miR-222 targets (20). Three hundred ten targets were obtained ([sup-](#)

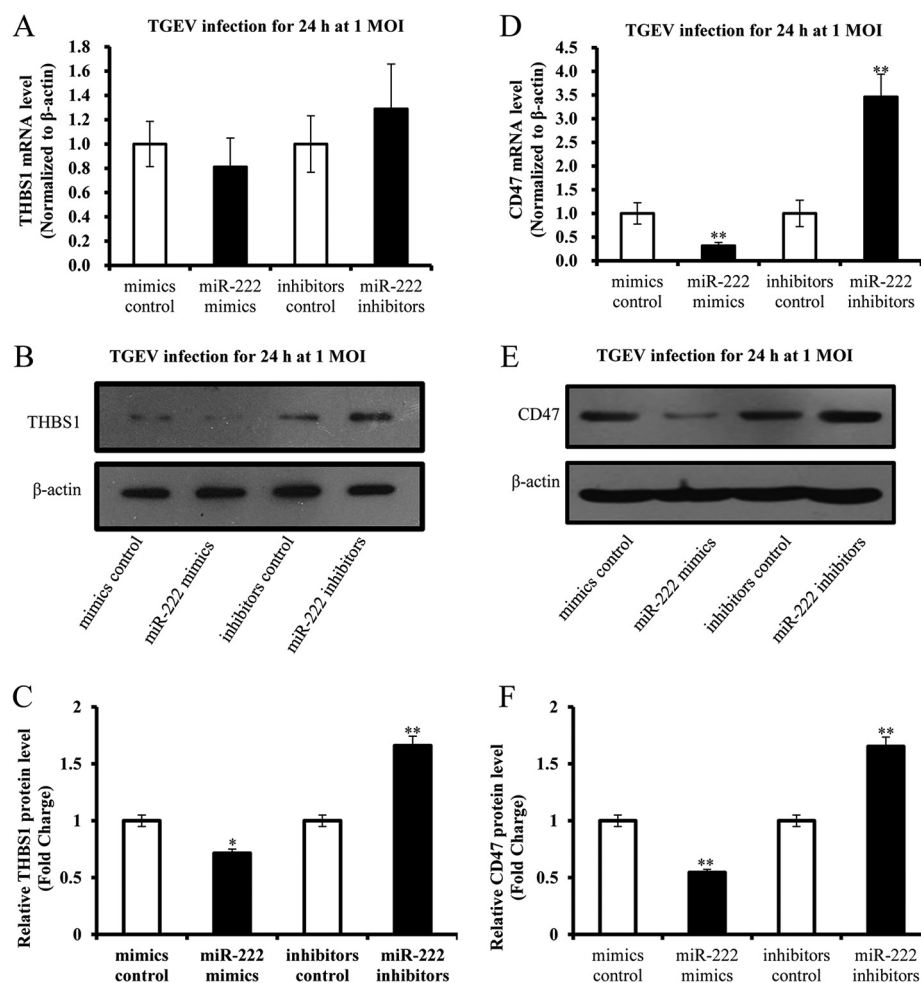


FIG. 7. Validation of differentially expressed proteins. *A*, The effect of miR-222 on mRNA level of THBS1; *B*, Expression of THBS1 was reduced by miR-222 mimics and promoted by miR-222 inhibitors; *C*, The effect of miR-222 on mRNA level of CD47; *D*, Expression of CD47 was downregulated by miR-222 mimics and upregulated by miR-222 inhibitors. Data represent mean \pm S.D. of three independent experiments. * $p < 0.05$ compared with the control. ** $p < 0.01$ compared with the control.

plemental S2) and searched against GO database to provide enrichment information on Biological Process, Molecular Function, and Cellular Component. GO enrichment of the 310 targets of miR-222 showed that 48.5% of targets were enriched in metabolic process and 24.2% of targets were involved in mitochondria in Cellular component (Fig. 1).

KEGG Pathway Enrichment Analysis of Differentially Expressed Proteins—KAAS, an online service tool of KEGG, was used to annotate the 310 targets of miR-222. Annotations were mapped on KEGG pathway database using KEGG mapper. KEGG enrichment analysis revealed the targets of miR-222 were primarily enriched in Peroxisome, PPAR signaling pathway, Biosynthesis of unsaturated fatty acids, and Fatty acid degradation (Fig. 2A). The mitochondria-related targets of miR-222 were mainly enriched in Fatty acid degradation, Peroxisome, PPAR signaling pathway, and Metabolic pathway (Fig. 2B).

miR-222 Decreased Mitochondrial Ca^{2+} Level and Increased MMP Level—To investigate the impact of miR-222 on mitochondrial dysfunction during TGEV infection, PK-15 cells were transfected with miR-222 mimics/miR-222 inhibitors and subsequently infected with TGEV or treated with medium

instead of TGEV, named MOCK infection. Mitochondrial Ca^{2+} level and MMP level were measured at 24 hpi. Overexpression and silence of miR-222 were successfully achieved by miR-222 mimics (Fig. 3A) and miRNA-222 inhibitors (Fig. 3B). Mitochondrial Ca^{2+} level was downregulated by miR-222 mimics and was upregulated by miR-222 inhibitors (Fig. 3C). MMP level was increased by miR-222 mimics and was decreased by miR-222 inhibitors (Fig. 3D). The results suggest that miR-222 counteracts TGEV-induced mitochondrial dysfunction in PK-15 cells.

Identification of 100 Differentially Expressed Proteins in TGEV-infected PK-15 Cells—To analyze the molecular mechanism of miR-222 in TGEV-induced mitochondrial dysfunction, relative protein quantification was performed. A total of 4209 proteins were detected and quantified (supplemental Fig. S3). When setting quantification ratio of >1.2 ($p < 0.05$) as upregulated threshold and <0.83 ($p < 0.05$) as downregulated threshold, 100 differentially expressed proteins were obtained, including 57 upregulated proteins and 43 downregulated proteins (Table I). Raw data of MS have been deposited to the ProteomeXchange Consortium via the PRIDE

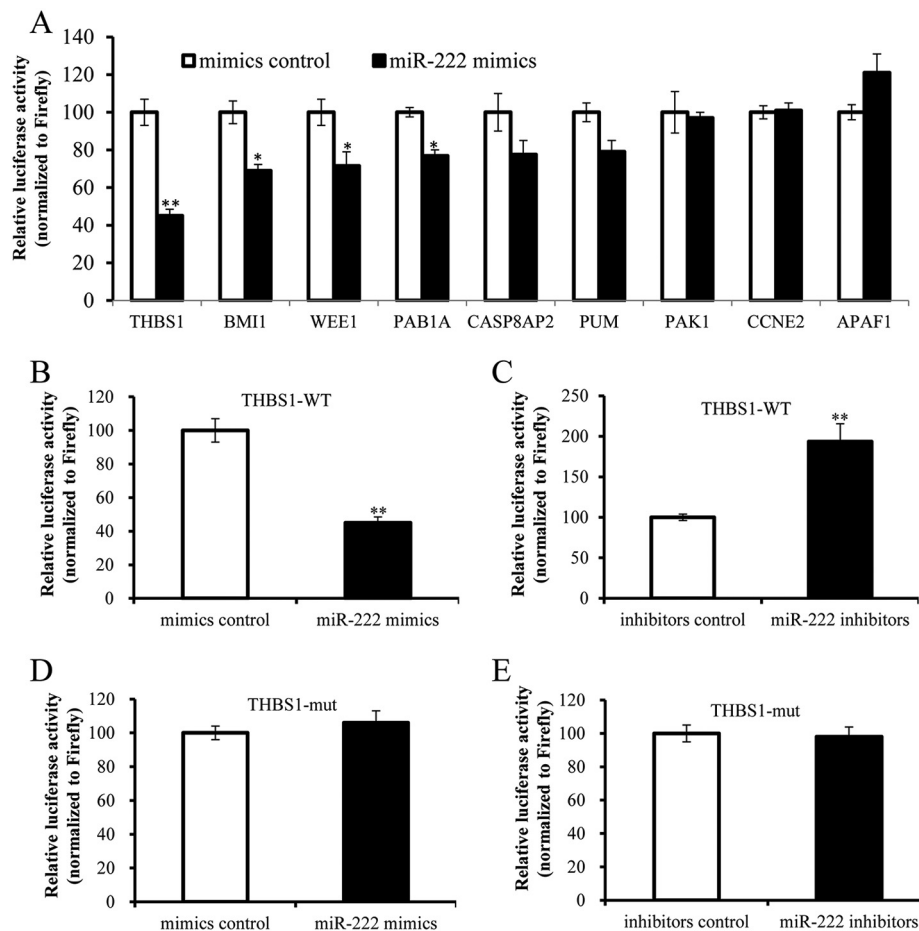


FIG. 8. THBS1 is the direct target of miR-222. A, The binding ability of miR-222 to 3' UTRs of 9 potential target genes; B and C, The binding ability of miR-222 to 3' UTR of THBS1 wildtype (THBS1-WT); D and E, The binding ability of miR-222 to mutant 3' UTR of THBS1 (THBS1-mut). Data represent means \pm S.D. of three independent experiments. * $p < 0.05$ compared with the control. ** $p < 0.01$ compared with the control.

partner repository with the data set identifier PXD010927 (<http://www.ebi.ac.uk/pride>).

GO Enrichment Analysis of the 100 Differentially Expressed Proteins—Subcellular localization of 100 differentially expressed proteins was analyzed by searching against Wolf Psort database (<https://wolfsort.hgc.jp/>). The result showed that the 100 differentially expressed proteins were localized at cytosol (35.0%), nuclear (23.0%), mitochondria (18.0%), extracellular (6.0%), plasma membrane (6.0%), endoplasmic reticulum (4.0%), and peroxisome (1.0%) (Fig. 4A). The 100 differentially expressed proteins were annotated by UniProt-GOA database and enriched by GO annotation based on three categories: Biological Process, Cellular Component, and Molecular Function. In Biological Process, the 100 differentially expressed proteins were primarily enriched in metabolic process. The Cellular component was mainly involved in intracellular (90.9%), intracellular part (86.0%), intracellular organelle (76.1%), and especially mitochondrial part (9.9%). In Molecular function, the 100 differentially expressed proteins were primarily enriched in anion binding (84.0%) and nucleotide binding (79.1%) (Fig. 4B).

KEGG Pathway Enrichment Analysis of Differentially Expressed Proteins—The 100 differentially expressed proteins were searched for functional enrichment by a KEGG database

search. The results showed that these proteins were mainly enriched in Ribosome, ECM-receptor interaction, Oxidative phosphorylation, and Focal adhesion (Fig. 5A). The mitochondria-related proteins were prevalently enriched in Oxidative phosphorylation and Mitochondrial ribosome (Fig. 5B). The differentially expressed proteins were used as an input list for the web-tool STRING to generate protein-protein interaction networks (Fig. 6). It is interesting that THBS1 interacts with CD47. THBS1 is predicted as one of the targets of miR-222.

Verification of Differentially Expressed Proteins by Western blotting and qRT-PCR—Relative quantitative proteomic analysis showed that miR-222 mimics downregulated expression of THBS1 and CD47. According to Protein-Protein interaction analysis of miR-222 targets, THBS1 is predicted the target of miR-222 and interacts with CD47. Moreover, THBS1 is related to regulate mitochondrial function (21, 22). Therefore, expression of THBS1 and CD47 were verified. The mRNA level of THBS1 was not influenced by miR-222 (Fig. 7A). The mRNA level of CD47 was reduced by miR-222 mimics and elevated by miR-222 inhibitors (Fig. 7C). Expression levels of THBS1 and CD47 were inhibited by miR-222 mimics and promoted by miR-222 inhibitors (Fig. 7B and 7D).

THBS1 is a Direct Target of miR-222—To identify the mitochondria-related target of miR-222, 3' UTRs of 9 mitochon-

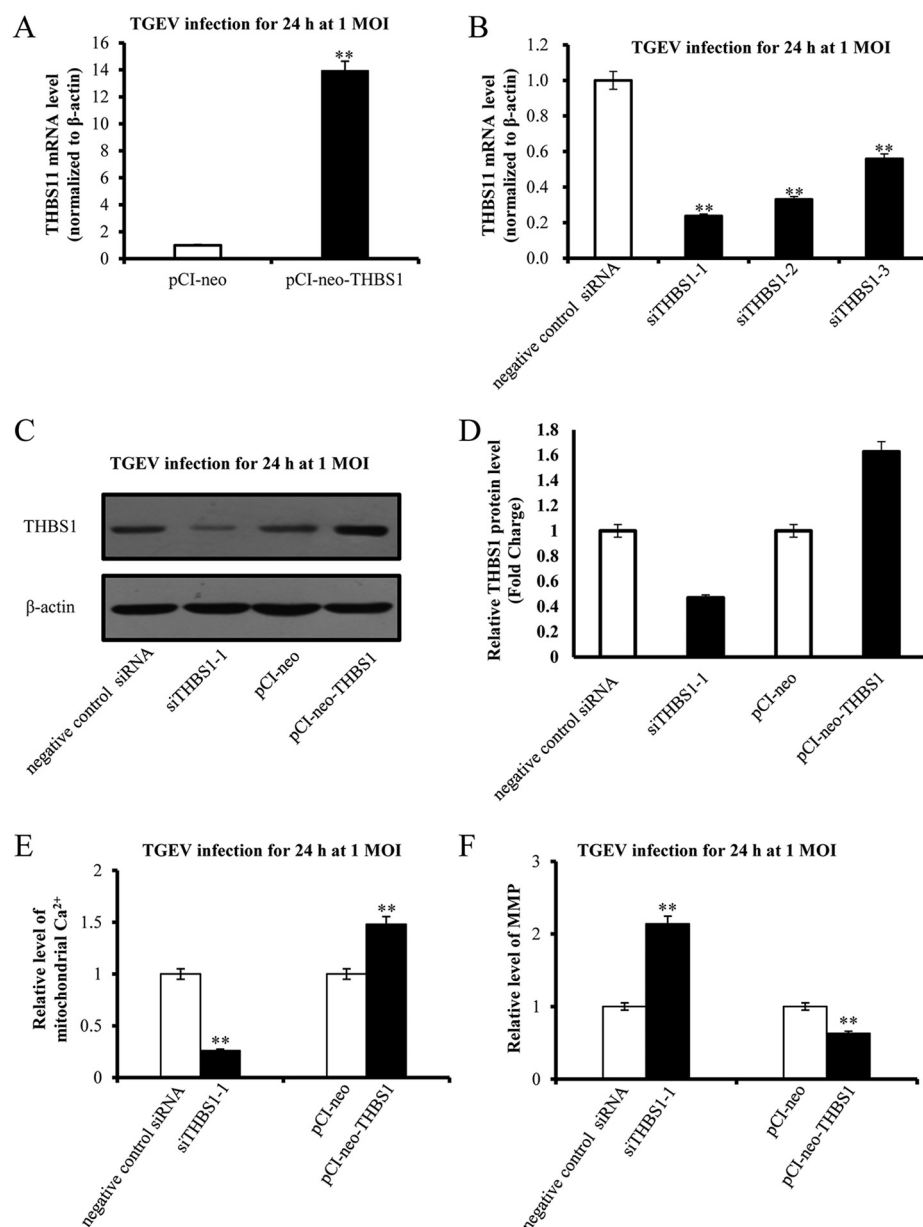


FIG. 9. The effect of THBS1 on TGEV-induced mitochondrial dysfunction. A, mRNA level of THBS1-1 caused by pCI-neo-THBS1; B, Silencing effects of THBS1's siRNAs at mRNA level; C, The effects of siTHBS1 and pCI-neo-THBS1 on expression of THBS1; D, Quantification of expression of THBS1 in response to siTHBS1 and pCI-neo-THBS1; E, The effect of THBS1 on mitochondrial Ca^{2+} level during TGEV infection; F, The effect of THBS1 on MMP level during TGEV infection. Data represent mean \pm S.D. of three independent experiments. * $p < 0.05$ compared with the control. ** $p < 0.01$ compared with the control.

dria-related targets, including THBS1, were respectively amplified and cloned into 3' UTR of Renilla luciferase of dual-luciferase reporter plasmid psiCHECK-2. The recombinants and miR-222 mimics/inhibitors were co-transfected into PK-15 cells. The luciferase activities were detected. The results showed that the Renilla luciferase activity of plasmid containing the 3' UTR of THBS1 was markedly lower than that of the control (normalized to Firefly luciferase activity) (Fig. 8A). To further confirm the direct binding between miR-222 and 3' UTR of THBS1, the mutated 3' UTR sequence of THBS1, in which miR-222 seed sequence was mutated, was cloned into the 3' UTR of Renilla luciferase to generate construction THBS1-mut. The constructs were respectively co-transfected into PK-15 cells with either miR-222 mimics or

inhibitors. The Renilla luciferase activity of THBS1-WT was reduced by miR-222 mimics and potentiated by miR-222 inhibitors (normalized to Firefly luciferase activity) (Fig. 8B and 8C). The Renilla luciferase activity of THBS1-mut was not affected by mimics and inhibitors of miR-222 (Fig. 8D and 8E). Moreover, the mRNA level of THBS1 was not changed by miR-222 mimics and miR-222 inhibitors (Fig. 7A). However, the protein level of THBS1 was reduced by miR-222 mimics and increased by miR-222 inhibitors (Fig. 7B). Taken together, our data identified that THBS1 was a direct target of miR-222.

Effects of THBS1 on Mitochondrial Ca^{2+} and MMP Levels—We demonstrated that miR-222 targeted THBS1 and reduced TGEV-induced mitochondrial dysfunction. So, we speculate that miR-222 might suppress TGEV-induced mito-

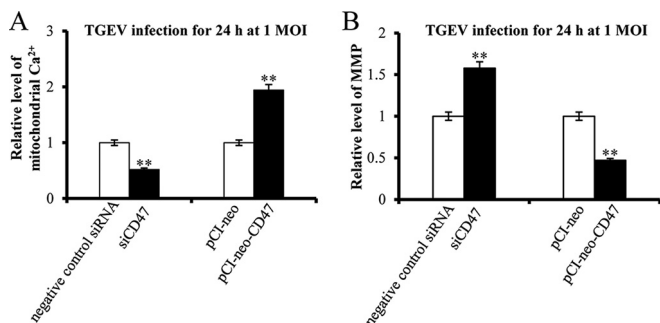


FIG. 10. **The effect of CD47 on TGEV-induced mitochondrial dysfunction.** A, The effect of CD47 on mitochondrial Ca²⁺ level during TGEV infection; B, The effect of CD47 on MMP level during TGEV infection. * *p* < 0.05 compared with the control. ** *p* < 0.01 compared with the control.

chondrial dysfunction via targeting THBS1. To identified that, THBS1 was knocked down by artificial siRNAs and overexpressed by pCI-neo-THBS1 (Fig. 9A, 9B, and 9C). Mitochondrial Ca²⁺ level was reduced by siTHBS1-1 and elevated by pCI-neo-THBS1 (Fig. 9D). MMP level was upregulated by siTHBS1-1 and downregulated by pCI-neo-THBS1 (Fig. 9E).

Effects of CD47 on Mitochondrial Ca²⁺ and MMP Levels—pCI-neo-CD47 was constructed to overexpress CD47. siRNAs of CD47 were design and synthesized (RiboBio, China). PK-15 cells were respectively transfected with pCI-neo-CD47 and siCD47 and subsequently infected with TGEV. Mitochondrial Ca²⁺ and MMP were tested. Mitochondrial Ca²⁺ was decreased by siCD47 and increased by pCI-neo-CD47 (Fig. 10A). MMP level was facilitated by siCD47 and reduced by pCI-neo-CD47 (Fig. 10B).

DISCUSSION

In this study, relative protein quantification was performed using TMT MS/MS to quantify proteome in presence of miR-222 mimics treatment. 100 differently expressed proteins were obtained, including 57 upregulated and 43 downregulated proteins. Based on bioinformatics analysis, miR-222 was linked to mitochondria, so we presumed that miR-222 might be involved in regulating TGEV-induced mitochondrial dysfunction. Our results indicate that miR-222 can attenuate TGEV-induced mitochondrial dysfunction by targeting THBS1 and downregulating CD47 (Fig. 11).

By quantitative proteomic analysis, 100 differentially expressed proteins were obtained. Subcellular localization and GO analysis of the 100 differentially expressed proteins showed that 18.0% proteins are located at mitochondria and prevaillingly enriched in metabolic process. Among the 100 differentially expressed proteins, many mitochondrial proteins are regulated by miR-222 during TGEV infection, including MRPL11, MRPL24, MRPS26, MRPL38, MRPL46, MRPL47, NDUFV1, NDUFS1, NDUFA13, NDUFC2, and NDUFB5. MRPL11, MRPL24, MRPS26, MRPL38, MRPL46, and MRPL47 are mammalian mitochondrial ribosomal proteins and contribute to synthesis of essential mitochondrial pro-

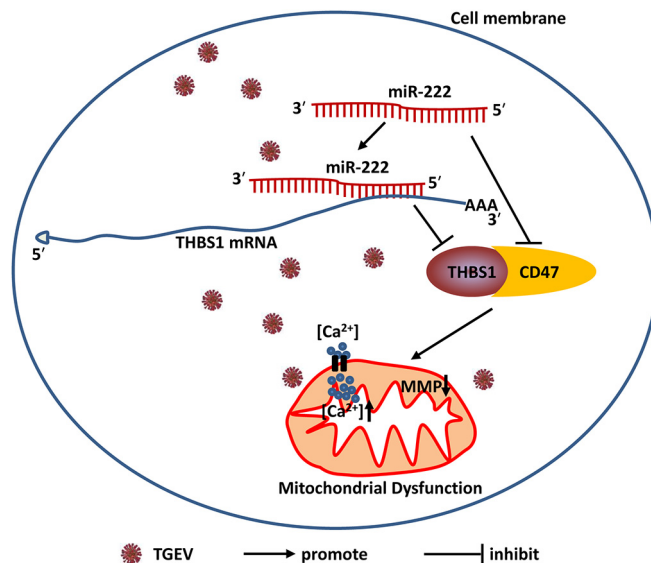


FIG. 11. **A model for miR-222 role in TGEV-induced mitochondrial dysfunction.**

teins (23, 24). NDUFV1, NDUFS1, NDUFA13, NDUFC2, and NDUFB5 are NADH-dehydrogenases of mitochondria (25). NADH-dehydrogenase is one of the most important enzyme of complex I (26). Results of KEGG pathway analysis reveal that these differentially proteins are involved in ribosome, ECM-receptor interaction, oxidative phosphorylation, pyruvate metabolism, glucagon signaling pathway, and fatty acid metabolism. Results of GO and KEGG analysis show that miR-222 might be primarily involved in regulation of mitochondrial function during TGEV infection.

Mitochondria are eukaryotic organelle and mainly involved in many metabolic processes, including metabolism of glucose, fat, protein, and nucleic acid (27–30). Mitochondrial dysfunction is a key reason in many pathogenic processes, including metabolism, cell death, autophagy, and viral infection (31, 32). It was reported that depletion of miR-222 damaged mitochondrial membrane potential, indicating that miR-222 functions as an inhibitor of mitochondrial dysfunction (33). In this present study, we found that miR-222 resulted in an increase of mitochondrial membrane potential. Mitochondria have ability to take up cytoplasmic Ca²⁺ to maintain calcium homeostasis. But, once excessive Ca²⁺ enters mitochondria, mitochondria will be damaged (34). Here, we observed that mitochondrial Ca²⁺ level was augmented by miR-222. Our data imply miR-222 might counteract TGEV-induced mitochondrial dysfunction. These results are consistent with the previous findings.

THBS1 is a secretive glycoprotein and involved in regulation of mitochondrial function. Knockout of THBS1 results in mitochondrial dysfunction in mice (21). THBS1 can prevent mitochondrial pathway of apoptosis from being triggered (35) and inhibits palmitate-induced release of mitochondrial cytochrome c, cleavage of capase-3, and apoptosis (36), indicat-

ing THBS1 plays a role in mitochondrial function. We demonstrated that THBS1 is a regulator of mitochondrial dysfunction during TGEV infection, being consistent with the previous reports.


CD47 is a cell-surface receptor and can bind to THBS1 to form a complex to modulate mitochondrial function (22, 37). THBS1 interacting with CD47 leads to mitochondrial dysfunction by disruption of the MMP (22). We found that CD47 and THBS1 promoted mitochondrial dysfunction during TGEV infection, indicating that interaction between CD47 and THBS1 play an important role in TGEV-induced mitochondrial dysfunction.

In conclusion, we found that proteome was changed by miR-222 during TGEV infection by quantitative proteomic analysis. Moreover, miR-222 played a role in decreasing mitochondrial Ca^{2+} level and increasing TGEV-reduced MMP in PK-15 cells by targeting THBS1 and suppressing CD47.

DATA AVAILABILITY

The mass spectrometry proteomics data have been deposited to the ProteomeXchange Consortium via the PRIDE partner repository with the dataset identifier PXD010927 (<http://www.ebi.ac.uk/pride>; Project accession: PXD010927).

* This work was supported by grants from Natural Science Foundation of China (Grant No. 31472167), China Postdoctoral Science Foundation (Grant No. 2015M570860), Key Research and Development Project in Shaanxi Province (Grant No. 2018ZDXM-NY-064), and Central Project of Major Agricultural Technology Promotion Funds (Grant No. K3360217060).

 This article contains supplemental Tables.

¶ To whom correspondence should be addressed: College of Veterinary Medicine, Northwest A&F University, Yangling, Shaanxi 712100, P.R. China. Tel.: +86-13892879237; Fax: +86-29-87091032; E-mail: dwtong@nwsuaf.edu.cn.

Author contributions: X.Z., X.S., and D.T. designed research; X.Z., X.S., X.B., Z.T., X.M., J.G., and Z.Z. performed research; X.Z., X.S., X.B., Z.Z., Q.D., Y.H., and D.T. analyzed data; X.Z., X.S., and X.B. wrote the paper; Z.T., X.M., Y.H., and D.T. contributed new reagents/analytic tools; X.Z. provided funding support.; D.T. provided funding.

REFERENCES

- Weiss, S. R., and Leibowitz, J. L. (2011) *Coronavirus Pathogenesis*. **81**, 85–164
- Zhao, X., Song, X., Bai, X., Fei, N., Huang, Y., Zhao, Z., Du, Q., Zhang, H., Zhang, L., and Tong, D. (2016) miR-27b attenuates apoptosis induced by transmissible gastroenteritis virus (TGEV) infection via targeting runt-related transcription factor 1 (RUNX1). *PeerJ* **4**, e1635
- Ding, Z., An, K., Xie, L., Wu, W., Zhang, R., Wang, D., Fang, Y., Chen, H., Xiao, S., and Fang, L. (2017) Transmissible gastroenteritis virus infection induces NF- κ B activation through RLR-mediated signaling. *Virology* **507**, 170–178
- Guo, L., Yu, H., Gu, W., Luo, X., Li, R., Zhang, J., Xu, Y., Yang, L., Shen, N., Feng, L., and Wang, Y. (2016) Autophagy Negatively Regulates Transmissible Gastroenteritis Virus Replication. *Sci. Rep.* **6**, 23864
- Ding, L., Xu, X., Huang, Y., Li, Z., Zhang, K., Chen, G., Yu, G., Wang, Z., Li, W., and Tong, D. (2012) Transmissible gastroenteritis virus infection induces apoptosis through FasL- and mitochondria-mediated pathways. *Vet. Microbiol.* **158**, 12–22
- Ding, L., Zhao, X., Huang, Y., Du, Q., Dong, F., Zhang, H., Song, X., Zhang, W., and Tong, D. (2013) Regulation of ROS in transmissible gastroenteritis virus-activated apoptotic signaling. *Biochem. Biophys. Res. Commun.* **442**, 33–37
- Zhong, Z., Umemura, A., Sanchez-Lopez, E., Liang, S., Shalpour, S., Wong, J., He, F., Boassa, D., Perkins, G., Ali, S. R., McGeough, M. D., Ellisman, M. H., Seki, E., Gustafsson, A. B., Hoffman, H. M., Diaz-Meco, M. T., Moscat, J., and Karin, M. (2016) NF- κ B restricts inflammasome activation via elimination of damaged mitochondria. *Cell* **164**, 896–910
- Kalogianni, D. P., Kalligiosfyri, P. M., Kyriakou, I. K., and Christopoulos, T. K. (2018) Advances in microRNA analysis. *Anal. Bioanal. Chem.* **410**, 695–713
- Balasubramaniam, M., Pandhare, J., and Dash, C. (2018) *Are microRNAs Important Players in HIV-1 Infection? An Update*. *Viruses* **10**, 110–145
- Moyano, A. L., Stepkowski, J., Wang, H., Son, K. N., Rapolti, D. I., Marshall, J., Elackattu, V., Marshall, M. S., Hebert, A. K., Reiter, C. R., Ulloa, V., Pituch, K. C., Givogri, M. I., Lu, Q. R., Lipton, H. L., and Bongarzone, E. R. (2018) microRNA-219 reduces viral load and pathologic changes in Theiler's virus-induced demyelinating disease. *Mol. Ther.* **26**, 730–743
- Bienertova-Vasku, J., Sana, J., and Slaby, O. (2013) The role of microRNAs in mitochondria in cancer. *Cancer Lett.* **336**, 1–7
- Wu, W., Chen, X., Yu, S., Wang, R., Zhao, R., and Du, C. (2018) microRNA-222 promotes tumor growth and confers radioresistance in nasopharyngeal carcinoma by targeting PTEN. *Mol. Med. Rep.* **17**, 1305–1310
- Song, X., Zhao, X., Huang, Y., Xiang, H., Zhang, W., and Tong, D. (2015) Transmissible gastroenteritis virus (TGEV) infection alters the expression of cellular microRNA species that affect transcription of TGEV gene 7. *Int. J. Biol. Sci.* **11**, 913–922
- Zhao, X., Bai, X., Guan, L., Li, J., Song, X., Ma, X., Guo, J., Zhang, Z., Du, Q., Huang, Y., and Tong, D. (2018) microRNA-4331 promotes transmissible gastroenteritis virus (TGEV)-induced mitochondrial damage via targeting RB1, upregulating interleukin-1 receptor accessory protein (IL1RAP), and activating p38 MAPK pathway in vitro. *Mol. Cell. Proteomics* **17**, 190–204
- Ding, L., Chen, G. D., Xu, X. G., and Tong, D. W. (2011) Isolation and identification of porcine transmissible gastroenteritis virus Shaanxi strain and sequence analysis of its N gene. *Chin. J. Vet. Med.* **47**, 9–11
- Livak, K. J., and Schmittgen, T. D. (2001) Analysis of relative gene expression data using real-time quantitative PCR and the 2- $\Delta\Delta$ CT method. *Methods* **25**, 402–408
- Cox, J., Matic, I., Hilger, M., Nagaraj, N., Selbach, M., Olsen, J. V., and Mann, M. (2009) A practical guide to the MaxQuant computational platform for SILAC-based quantitative proteomics. *Nat. Protoc.* **4**, 698–705
- Vizcaino, J. A., Csordas, A., Del-Toro, N., Dianes, J. A., Griss, J., Lavidas, I., Mayer, G., Perez-Riverol, Y., Reisinger, F., Ternent, T., Xu, Q. W., Wang, R., and Hermjakob, H. (2016) 2016 update of the PRIDE database and its related tools. *Nucleic Acids Res.* **44**, 11033
- Szklarczyk, D., Franceschini, A., Kuhn, M., Simonovic, M., Roth, A., Minguez, P., Doerks, T., Stark, M., Muller, J., Bork, P., Jensen, L. J., and Von Mering, C. (2011) The STRING database in 2011: functional interaction networks of proteins, globally integrated and scored. *Nucleic Acids Res.* **39**, D561–D568
- Song, X., Zhao, X., Huang, Y., Xiang, H., Zhang, W., and Tong, D. (2015) Transmissible Gastroenteritis Virus (TGEV) Infection alters the expression of cellular microRNA species that affect transcription of TGEV gene 7. *Int. J. Biol. Sci.* **11**, 913–922
- Soto-Pantoja, D. R., Sipes, J. M., Martin-Manso, G., Westwood, B., Morris, N. L., Ghosh, A., Emenaker, N. J., and Roberts, D. D. (2016) Dietary fat overcomes the protective activity of thrombospondin-1 signaling in the Apc(Min/+) model of colon cancer. *Oncogenesis*, **5**, e230
- Frazier, E. P., Isenberg, J. S., Shiva, S., Zhao, L., Schlesinger, P., Dimitry, J., Abu-Asab, M. S., Tsokos, M., Roberts, D. D., and Frazier, W. A. (2011) Age-dependent regulation of skeletal muscle mitochondria by the thrombospondin-1 receptor CD47. *Matrix Biol.* **30**, 154–161
- Cavdar Koc, E., Burkhart, W., Blackburn, K., Moseley, A., and Spremulli, L. L. (2001) The small subunit of the mammalian mitochondrial ribosome. Identification of the full complement of ribosomal proteins present. *J. Biol. Chem.* **276**, 19363–19374
- Kenmochi, N., Suzuki, T., Uechi, T., Magoori, M., Kuniba, M., Higa, S., Watanabe, K., and Tanaka, T. (2001) The human mitochondrial ribosomal protein genes: mapping of 54 genes to the chromosomes and implications for human disorders. *Genomics*. **77**, 65–70
- Hirst, J. (2013) Mitochondrial Complex I. *Annu. Rev. Biochem.* **82**, 551–575

26. Liu, C., Fetterman, J. L., Liu, P., Luo, Y., Larson, M. G., Vasan, R. S., Zhu, J., and Levy, D. (2018) Deep sequencing of the mitochondrial genome reveals common heteroplasmic sites in NADH dehydrogenase genes. *Hum. Genet.* **137**, 203–213
27. Lee, C., Kim, K. H., and Cohen, P. (2016) MOTS-c: A novel mitochondrial-derived peptide regulating muscle and fat metabolism. *Free Radic. Biol. Med.* **100**, 182–187
28. Desler, C., Lykke, A., and Rasmussen, L. J. (2010) The effect of mitochondrial dysfunction on cytosolic nucleotide metabolism. *J. Nucleic Acids* **47**, 1230–1243
29. Samardzic, K., and Rodgers, K. J. (2017) Oxidised protein metabolism: recent insights. *Biol. Chem.* **398**, 1165–1175
30. Heier, C., and Haemmerle, G. (2016) Fat in the heart: The enzymatic machinery regulating cardiac triacylglycerol metabolism. *Biochim. Biophys. Acta* **1861**, 1500–1512
31. Guo, R., Davis, D., and Fang, Y. (2018) Intercellular transfer of mitochondria rescues virus-induced cell death but facilitates cell-to-cell spreading of porcine reproductive and respiratory syndrome virus. *Virology* **517**, 122–134
32. Lindqvist, L. M., Frank, D., McArthur, K., Dite, T. A., Lazarou, M., Oakhill, J. S., Kile, B. T., and Vaux, D. L. (2018) Autophagy induced during apoptosis degrades mitochondria and inhibits type I interferon secretion. *Cell Death Differ.* **25**, 782–794
33. Zhang, C. Z., Zhang, J. X., Zhang, A. L., Shi, Z. D., Han, L., Jia, Z. F., Yang, W. D., Wang, G. X., Jiang, T., You, Y. P., Pu, P. Y., Cheng, J. Q., and Kang, C. S. (2010) MiR-221 and miR-222 target PUMA to induce cell survival in glioblastoma. *Mol. Cancer* **9**, 229
34. Wang, H. W., Liu, J., Zhao, J., Lin, L., Zhao, W. P., Tan, P. P., Tian, W. S., and Zhou, B. H. (2018) Ca(2+) metabolic disorder and abnormal expression of cardiac troponin involved in fluoride-induced cardiomyocyte damage. *Chemosphere* **201**, 564–570
35. Cunha, D. A., Cito, M., Grieco, F. A., Cosentino, C., Danilova, T., Ladriere, L., Lindahl, M., Domanskyi, A., Bugliani, M., Marchetti, P., Eizirik, D. L., and Cnop, M. (2017) Pancreatic beta-cell protection from inflammatory stress by the endoplasmic reticulum proteins thrombospondin 1 and mesencephalic astrocyte-derived neurotrophic factor (MANF). *J. Biol. Chem.* **292**, 14977–14988
36. Cunha, D. A., Cito, M., Carlsson, P. O., Vanderwinden, J. M., Molkentin, J. D., Bugliani, M., Marchetti, P., Eizirik, D. L., and Cnop, M. (2016) Thrombospondin 1 protects pancreatic beta-cells from lipotoxicity via the PERK-NRF2 pathway. *Cell Death Differ.* **23**, 1995–2006
37. Jeanne, A., Boulagnon-Rombi, C., Devy, J., Theret, L., Fichel, C., Bouland, N., Diebold, M. D., Martiny, L., Schneider, C., and Dedieu, S. (2016) Matricellular TSP-1 as a target of interest for impeding melanoma spreading: towards a therapeutic use for TAX2 peptide. *Clin. Exp. Metastasis* **33**, 637–649